

Hybrid Position and Orientation Estimation for Visible Light Systems in the Presence of Prior Information on the Orientation

Shengqiang Shen¹, Shiyin Li¹, and Heidi Steendam², *Senior Member, IEEE*

Abstract—Visible light communication (VLC) is seen as a potential access option for fifth-generation (5G) wireless communication (Wang *et al.*, 2014) and (Ayyash *et al.*, 2016) and beyond 5G (Strinati *et al.*, 2019). A reliable VLC system benefits from an accurate estimate of the receiver’s position and orientation. In many cases, the orientation of the receiver is estimated with an external orientation estimation device. However, these devices generally suffer from drift and misalignment, causing an uncertainty in the orientation presented to the receiver. Hence, the external device can only provide a probability distribution of the orientation to the position estimator, which can be used as prior information for the position estimation. Since the orientation of a receiver greatly affects the performance of a visible light system, the orientation uncertainty will degrade the performance of standard positioning algorithms, implying it should be taken into account when designing a robust positioning algorithm. In this paper, we design an received signal strength (RSS)-based hybrid position and orientation estimation algorithm using the hybrid maximum likelihood (ML)/maximum a posteriori (MAP) (HyMM) principle for a multiple LEDs - multiple photodiodes (PDs) (MLMP) system to take into account the presence of prior information on the orientation. The proposed HyMM estimator is compared with three existing estimators, i.e., the simultaneous position and orientation (SPO) estimator, the misspecified maximum likelihood (MML) estimator and the first-order-approximation-based positioning algorithm, subject to the orientation uncertainty. Further, in order to analytically assess the performance of the proposed estimator, the theoretical lower bound on the mean squared error (MSE), i.e. the hybrid Cramér-Rao bound (HCRB) for HyMM is derived. Computer simulations show an asymptotic tightness between the performance of the estimator and its associated theoretical lower bound.

Index Terms—Visible light system, prior information on the orientation, position and orientation estimation, multiple LEDs and multiple PDs, hybrid ML/MAP estimator, hybrid Cramér-Rao bound.

Manuscript received 9 November 2020; revised 22 October 2021; accepted 25 January 2022. Date of publication 8 February 2022; date of current version 12 August 2022. This work was supported in part by the Belgian Research Councils The Research Foundation – Flanders (FWO) and National Fund for Scientific Research (FNRS) under Excellence of Science (EOS) Grant 30452698 and in part by the Flemish Government (AI Research Program). The work of Shiyin Li was supported in part by the National Natural Science Foundation of China under Grant 61771474. The associate editor coordinating the review of this article and approving it for publication was M. Uysal. (Corresponding author: Shengqiang Shen.)

Shengqiang Shen and Shiyin Li are with the School of Information and Control Engineering, China University of Mining and Technology, Xuzhou 221116, China (e-mail: shengqiang.shen@outlook.com; lishiyin@cumt.edu.cn).

Heidi Steendam is with the Telecommunications and Information Processing Department, Ghent University/IMEC, 9000 Ghent, Belgium (e-mail: heidi.steendam@ugent.be).

Color versions of one or more figures in this article are available at <https://doi.org/10.1109/TWC.2022.3148169>.

Digital Object Identifier 10.1109/TWC.2022.3148169

I. INTRODUCTION

VISIBLE light communication (VLC) is seen as a potential access option for fifth-generation (5G) wireless communication [1], [2] and beyond 5G [3]. Compared to radio frequency (RF)-based solutions, communication systems based on visible light have many advantages. Due to their long life expectancy and cost effectiveness [4], LEDs are gradually replacing traditional light sources for lighting, implying they are becoming ubiquitously available. It also suffers less from interference from other sources, as light is blocked by opaque walls. VLC systems can coexist with lighting systems, and can safely be used in situations where interference from RF sources is harmful. The receiver of a visible light system consists of optical sensors, e.g. an image sensor [5]–[8] or photo diodes (PDs) [9]–[13]. As – compared to an image sensor – PD consume less energy and can detect signals that are modulated at higher frequencies, most recent works focus on receivers consisting of one or more PDs. Especially the PD array, consisting of multiple PDs, is gaining interest, as the designer has the ability to increase the receiver’s field-of-view (FOV) and angular diversity by tilting the PDs in the array or using apertures [10]–[12], resulting in an improvement of the performance. However, the visible light channel is largely sensitive to the distance and angle with respect to the transmitter. Therefore, a high-precision position and/or orientation estimate benefits reliable VLC systems.

In a VLC-based positioning – or visible light positioning (VLP) – system, most position and orientation related information is contained in the line-of-sight (LOS) link. If not properly addressed for, changes in the orientation may severely affect system’s performance. Most of the early works on VLP neglect the effect of orientation and assume that the receiver is parallel to the ceiling [14]–[16]. Later works considered two approaches to deal with the unknown orientation. In the first approach, the estimator tries to simultaneously estimate the position and orientation from the observed light signal only [17]–[20], while in the second approach, an external device is used to determine the orientation of the receiver [21], [22]. Both approaches have drawbacks. On the one hand, a simultaneous position and orientation (SPO) estimator not only requires a suitable receiver structure that can be exploited to provide a coarse orientation estimate, but also it neglects useful prior information about the orientation that could be obtained from an external device. On the other hand, in most cases, the external orientation estimation device is a Micro-Electro-Mechanical System (MEMS)-based

inertial measurement unit (IMU), as the cost and power consumption of such devices is low. The drawback of using these devices is their low accuracy, i.e. they suffer from severe biases and drift problems, especially when the receiver, which is carried by a user or attached to a carrier, experiences some random movement. Consequently, even if the receiver determines its orientation with an external orientation estimation device, the estimated orientation is subject to noise and orientation errors, meaning the instantaneous orientation is not perfectly known. Existing positioning algorithms extracting the orientation information from an external device often neglect the uncertainty generated by the external device and assume the orientation is perfectly estimated. In such a situation, the maximum likelihood estimator tries to estimate the position based on a misspecified model, i.e. in which the orientation is considered as uncertainty-free instead of satisfying some random process. In the following, we refer to this type of estimator as the misspecified maximum likelihood (MML) estimator [23]. For example, the algorithm from [9],¹ which in this paper is used to compare with the proposed estimator, and therefore is evaluated subject to the orientation uncertainty, can be considered as a MML estimator.

As this orientation uncertainty largely affects the positioning performance of state-of-the-art algorithms, it should be taken into account in the design of a positioning algorithm. To the best of our knowledge, there are only a few works [24], [25] on estimators taking into account the presence of prior information on the orientation. In [24], the authors derive a theoretical bound to analyze the performance of a receiver with a single PD. The orientation of the PD is represented by its normal vector. The drawback of this representation is that it describes a rotation with two degrees of freedom only, implying it can not reflect the heading direction and limits the extension of the bound for the receiver with a PD array [20]. Therefore, a more general representation of the orientation is required, allowing to describe the orientation with three degrees of freedom, e.g. by using the rotation matrix description. In our previous work [25], we analyzed the characteristics of the received signal strength subject to the orientation uncertainty, using this rotation matrix description, for a receiver consisting of a single PD. Based on a first-order approximated likelihood function, we designed for this receiver an RSS-based position estimator using the maximum likelihood principle. The resulting estimator outperforms state-of-the-art position estimators not taking into account orientation uncertainty. However, this approach cannot be extended effectively to the receiver consisting of a PD array, as not only the approach used in [25] is a positioning only algorithm, i.e., it treats the orientation as a nuisance parameter, but also applying this approach to a PD array system would result in biased estimates due to the approach's inconsistency. Therefore, in this paper, we consider a different approach, where we combine the prior information on the orientation

¹Note that the estimator [9] is originally designed for a receiver with a single PD and under the assumption that the receiver is parallel to the ceiling. However, the extension to a receiver with multiple PDs and perfectly known orientation is straightforward.

TABLE I
COMPARISON OF STATE-OF-THE-ART ESTIMATORS

Estimator	Features
MML [9]	Extracts the orientation information from an external device and neglects the uncertainty generated by the external device, assuming the orientation is perfectly estimated.
AP1st [25]	Treats the orientation as a nuisance parameter, and applies an approximation to the likelihood function.
SPO [20]	Neglects useful prior information about the orientation that could be obtained from an external device

from the noisy external device with that of the received optical signal to jointly estimate the position and orientation using the principle of hybrid maximum likelihood (ML)/maximum a posteriori (MAP) estimation (HyMM) [26], [27]. The performance of this HyMM algorithm will be compared with the performance of the three state-of-the-art algorithms mentioned above, i.e. the MML estimator, which is the estimator from [9] evaluated in the presence of orientation uncertainty, the simultaneous positioning and orientation (SPO) algorithm from [20], and the first-order-approximation-based positioning (AP1st) algorithm from [25]. These state-of-the-art algorithms are summarized in Tab. I. Further, the performance of the algorithms will be compared with a theoretical lower bound. The main contributions of this paper are as follows:

1) We first generalize the system model from [25], that includes orientation uncertainty for a single PD, to the case with multiple PDs. The resulting system model, from which the estimator will be derived, takes into account the received power of the multiple LEDs - multiple PDs (MLMP) system, as well as the estimated orientation and its uncertainty from the external device. The aim is to jointly estimate the position and orientation from the received light signal, and the observed orientation and its distribution. To this end, we propose an RSS-based hybrid position and orientation estimation algorithm using the principle of HyMM estimation, where the distribution of the orientation serves as prior information. The resulting HyMM estimator is then converted to a non-linear least squares (NLS) problem, which is easily solved using the Gauss-Newton algorithm on manifolds.

2) To compare the performance of the proposed HyMM estimator with the state-of-the-art algorithms MML [9], SPO [20], and AP1st [25], we not only perform Monte-Carlo simulations for the different algorithms, but also compare the performance of the algorithm with a theoretical lower bound. In this paper, we derive the hybrid Cramér-Rao bound (HCRB), which jointly bounds errors in both the position vector and the rotation matrix. In particular, in order to measure the error in the estimated rotation matrix, the intrinsic CRB on $SO(3)$ is utilized. The tightness of the bound is evaluated in this paper. By properly exploiting the prior information on orientation, our proposed method outperforms these baseline methods.

The rest of the paper is organized as follows. The channel gain model and received power are presented in Section II. The model of orientation uncertainty from an external device is provided in this section as well. The RSS-based hybrid position and orientation estimation algorithm using the hybrid ML/MAP principle is presented in Section III.

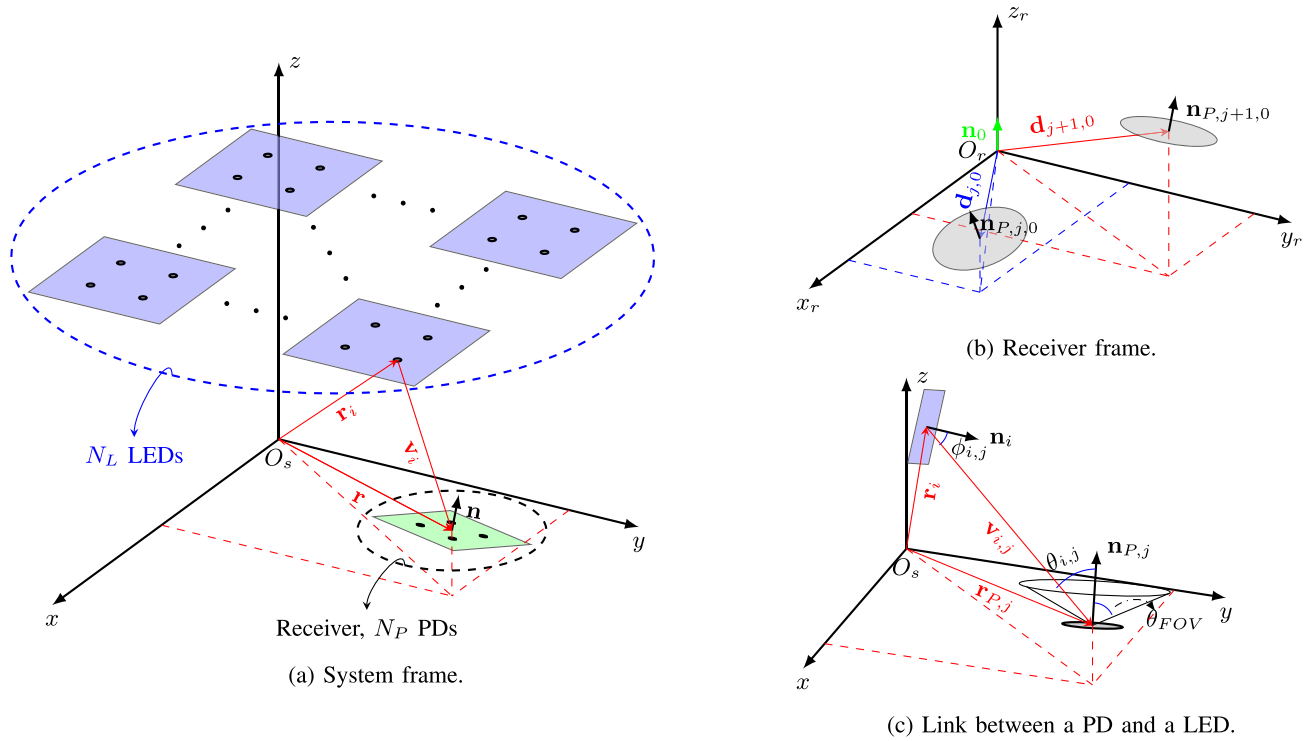


Fig. 1. System model.

Subsequently, the expression for the theoretical bound is derived in Section IV. Numerical results comparing the proposed algorithm with state-of-the-art algorithms, and the comparison with the theoretical lower bound, are given in Section V. Finally, some concluding remarks are given in Section VI.

Notation: Scalars are denoted in italic, e.g., x . Lower case boldface indicates a column vector, e.g., \mathbf{x} . Upper case boldface denotes a matrix or a set, e.g., \mathbf{X} , with \mathbf{I}_N representing an $N \times N$ identity matrix, and $\mathbf{0}_{N \times M}$ representing an $N \times M$ zero matrix. Matrix transpose, and inverse are indicated by superscript T , and -1 , respectively. The Euclidean norm is denoted by $\|\cdot\|$, while $\|\mathbf{x}\|_{\Sigma}^2 = \mathbf{x}^{\text{T}} \Sigma^{-1} \mathbf{x}$ is the squared Mahalanobis distance of \mathbf{x} with respect to matrix Σ . The expectation operator is denoted by $E\{\cdot\}$, and the set of all real numbers is denoted by \mathbb{R} . $\nabla_{\mathbf{x}} = \partial/\partial \mathbf{x}$ denotes the Del operator, and $\Pi(\cdot)$ is the rectangular function defined as

$$\Pi(x) \triangleq \begin{cases} 1, & |x| \leq 1. \\ 0, & |x| > 1. \end{cases} \quad (1)$$

The group of all rotation matrices, i.e., the special orthogonal group, is denoted by $SO(3)$, and the associated Lie algebra is denoted by $\mathfrak{so}(3)$. The operator $(\cdot)^{\wedge}$ converts the vector $\mathbf{x} = [x_1, x_2, x_3]^{\text{T}}$ into $\mathbf{x}^{\wedge} = \begin{bmatrix} 0 & -x_3 & x_2 \\ x_3 & 0 & -x_1 \\ -x_2 & x_1 & 0 \end{bmatrix} \in \mathfrak{so}(3)$, while the operator of $(\cdot)^{\vee}$ is the inverse operator of $(\cdot)^{\wedge}$.

II. SYSTEM DESCRIPTION

A. System Model

In this paper, we consider a system containing N_L LEDs and a VLP receiver containing N_P bare PDs mounted on the

receiver, as shown in Fig. 1. We assume that the i^{th} LED of the system has coordinates $\mathbf{r}_i \in \mathbb{R}^{3 \times 1}$ and normal $\mathbf{n}_i \in \mathbb{R}^{3 \times 1}$, i.e. the direction in which the LED is radiating, and that the coordinates and normals of the LED are known by the receiver. Since all PDs move and rotate rigidly with the receiver, i.e. their relative distances and orientations are preserved, the coordinates and orientations of all PDs are first defined in the frame of the receiver and then transformed into the frame of the system. In the frame of the receiver, shown in Fig. 1b, the coordinates of the j^{th} PD are specified by a relative vector $\mathbf{d}_{j,0}$ to the origin O_r (the centroid of the receiver), while the normal of the j^{th} PD is defined by a rotation matrix $\mathbf{R}_{P,j} \in SO(3)$ with respect to the normal vector \mathbf{n}_0 to the receiver plane, i.e. $\mathbf{n}_{P,j,0} = \mathbf{R}_{P,j} \mathbf{n}_0$. In the frame of the system, the receiver has coordinates \mathbf{r} , i.e. the position of the centroid of the receiver, and orientation $\mathbf{R} \in SO(3)$. Then the normal of the receiver is given by $\mathbf{n} = \mathbf{R} \mathbf{n}_0$. The position and the normal of the j^{th} PD are respectively expressed by $\mathbf{r}_{P,j} = \mathbf{r} + \mathbf{d}_j$ and $\mathbf{n}_{P,j} = \mathbf{R} \mathbf{n}_{P,j,0}$, where $\mathbf{d}_j = \mathbf{R} \mathbf{d}_{j,0}$ is the relative vector to \mathbf{r} .

B. Channel Gain and Received Power

Defining the vector $\mathbf{v}_i = \mathbf{r} - \mathbf{r}_i$ as the vector between the i^{th} LED and the receiver centroid, the incidence vector between the i^{th} LED and the j^{th} PD of the receiver can be written as $\mathbf{v}_{i,j} = \mathbf{v}_i + \mathbf{d}_j$ as shown in Fig. 1c. Using this definition, we find the distance $v_{i,j}$ between the i^{th} LED and the j^{th} PD, the radiation angle $\phi_{i,j}$, i.e. the angle between $\mathbf{v}_{i,j}$ and the normal \mathbf{n}_i of the LED, and the incidence angle $\theta_{i,j}$, i.e. the angle between $\mathbf{v}_{i,j}$ and the normal \mathbf{n} of the receiver:

$$v_{i,j} = \|\mathbf{v}_{i,j}\|, \quad (2)$$

$$\cos(\phi_{i,j}) = \frac{\mathbf{n}_i^T \mathbf{v}_{i,j}}{\|\mathbf{v}_{i,j}\|} = \frac{\mathbf{n}_i^T (\mathbf{v}_i + \mathbf{d}_j)}{\|\mathbf{v}_i + \mathbf{d}_j\|}, \quad (3)$$

$$\cos(\theta_{i,j}) = -\frac{\mathbf{n}_i^T \mathbf{v}_{i,j}}{\|\mathbf{v}_{i,j}\|} = -\frac{\mathbf{n}_i^T (\mathbf{v}_i + \mathbf{d}_j)}{\|\mathbf{v}_i + \mathbf{d}_j\|}. \quad (4)$$

The channel gain corresponding to the LOS component of the i^{th} LED and j^{th} PD is given by [28]:

$$h_{i,j} = \frac{(\gamma + 1) A_j}{2\pi v_{i,j}^2} \cos^\gamma(\phi_{i,j}) \cos(\theta_{i,j}) \Pi \times \left(\frac{\theta_{i,j}}{\theta_{FOV}} \right) \Pi \left(\frac{\phi_{i,j}}{\phi_{FOV}} \right), \quad (5)$$

where A_j is area of the j^{th} PD (in m^2), θ_{FOV} is the FOV of the PD, the Lambertian order of the LEDs equals γ . The factor $\Pi(\theta_{i,j}/\theta_{FOV}) \Pi(\phi_{i,j}/\phi_{FOV})$ in (5) implies that a PD can detect the light only when the LED is within its FOV, and the PD itself is within the FOV of the LED, i.e. when $0 \leq \theta_{i,j} \leq \theta_{FOV}$ and $0 \leq \phi_{i,j} \leq \phi_{FOV}$.

Taking into account (2)–(4), (5) can be rewritten as [20]

$$h_{i,j} = C_{i,j} \frac{(\mathbf{n}_i^T (\mathbf{v}_i + \mathbf{R} \mathbf{d}_{j,0}))^\gamma}{\|\mathbf{v}_i + \mathbf{R} \mathbf{d}_{j,0}\|^{\gamma+3}} (\mathbf{R} \mathbf{n}_{P,j,0})^T (\mathbf{v}_i + \mathbf{R} \mathbf{d}_{j,0}), \quad (6)$$

where $C_{i,j} = \frac{-(\gamma+1)A_j\Pi_{i,j}}{2\pi}$ and $\Pi_{i,j} = \Pi(\theta_{i,j}/\theta_{FOV}) \Pi(\phi_{i,j}/\phi_{FOV})$.

We assume a proper multiplexing protocol is used, e.g. frequency-division multiplexing (FDM) [12], time-division multiplexing (TDM) [29] or color-division multiplexing (CDM) [30], so that each PD is able to separate the signals from the different LEDs. Then the total observation consists of the RSS values from every PD-LED pair. Let us define the $N_L N_P \times 1$ vector $\mathbf{y} = [\mathbf{y}_1^T, \dots, \mathbf{y}_{N_P}^T]^T$ as the vector of observations, with $\mathbf{y}_j = [y_{1,j}, \dots, y_{N_L,j}]^T$, we obtain

$$\mathbf{y} = \mathbf{h} + \mathbf{w}, \quad (7)$$

where the $N_L N_P \times 1$ vector \mathbf{h} is defined as $\mathbf{h} = [\mathbf{h}_1^T, \dots, \mathbf{h}_{N_P}^T]^T$ with $\mathbf{h}_j = R_{p,j} [P_{t,1} h_{1,j}, \dots, P_{t,N_L} h_{N_L,j}]^T$, $P_{t,i}$ is the power transmitted by the i^{th} LED and $R_{p,j}$ is the responsivity of the j^{th} PD. The $N_L N_P \times 1$ vector \mathbf{w} models the shot and thermal noise [28], [31]. Although the shot noise is impulsive in nature, for sufficiently high intensity ambient light, the shot noise can be approximated by a Gaussian random variable thanks to the central limit theorem. Further, considering that the thermal noise is Gaussian distributed, the noise \mathbf{w} can be represented by a zero-mean multivariate Gaussian random variable [28], [31]–[33] with covariance matrix $\Sigma_{\mathbf{w}} = \sigma_w^2 \mathbf{I}_{N_L N_P}$.

C. Model of Orientation Uncertainty

In this section, we will discuss the model that will be used for the orientation uncertainty. The estimate $\tilde{\mathbf{R}} \in SO(3)$ of the rotation matrix \mathbf{R} , obtained with the external device, is modeled by $\tilde{\mathbf{R}} = \mathbf{R}_\epsilon \cdot \mathbf{R}$, where $\mathbf{R}_\epsilon \in SO(3)$ represents the random error component contained in the estimation. According to Euler's rotation theorem [34], the random rotation can be expressed as [35]–[38]

$$\mathbf{R}_\epsilon = \exp(\epsilon^\wedge) \quad (8)$$

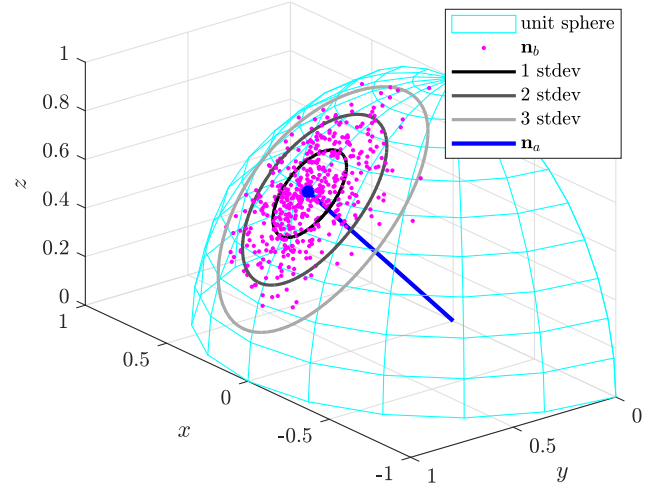


Fig. 2. Distribution of $\mathbf{n}_b = \mathbf{R}_\epsilon \mathbf{n}_a$.

where the skew-symmetric matrix ϵ^\wedge is constructed from the vector $\epsilon = [\epsilon_x \ \epsilon_y \ \epsilon_z]^T$ using the operator $(\cdot)^\wedge$. Physically, ϵ is the axis-angle representation of \mathbf{R}_ϵ and equation (8) is equivalent to Rodrigues' rotation formula that converts the axis-angle representation to the rotation matrix representation. Consequently, \mathbf{R}_ϵ realizes the rotation that rotates the rigid object around the unit axis of $\epsilon/\|\epsilon\|$ by an angle $\|\epsilon\|$. The distribution of \mathbf{R}_ϵ is specified by the rotation vector ϵ , which is assumed to be zero-mean Gaussian [25]. To illustrate the effect of a random rotation \mathbf{R}_ϵ , Fig. 2 shows the impact of \mathbf{R}_ϵ on a unit vector $\mathbf{n}_b = \mathbf{R}_\epsilon \mathbf{n}_a$, where \mathbf{n}_a is constant. The sampled \mathbf{n}_b (magenta dots) are concentrated around \mathbf{n}_a (the blue dot) and distributed on the unit sphere (the cyan mesh). The contours show the first 3 standard deviations of ϵ mapped to \mathbf{n}_b .

By left multiplying $\tilde{\mathbf{R}}$ with \mathbf{R}_ϵ^T , we have $\mathbf{R} = \mathbf{R}_\epsilon^T \tilde{\mathbf{R}}$, which induces the PDF of \mathbf{R} conditioned on $\tilde{\mathbf{R}}$, i.e., $p(\mathbf{R}|\tilde{\mathbf{R}})$. This PDF gives the probability distribution of true orientation \mathbf{R} given an estimate $\tilde{\mathbf{R}}$, and \mathbf{R}_ϵ^T models the uncertainty in the orientation estimate $\tilde{\mathbf{R}}$. Therefore, $p(\mathbf{R}|\tilde{\mathbf{R}})$ will serve as prior information about the orientation in the position estimator that uses the light signal. It can be seen that $p(\mathbf{R}|\tilde{\mathbf{R}})$ is specified by $p(\mathbf{R}_\epsilon^T)$, which is coupled with $p(\mathbf{R}_\epsilon)$ and determined by the PDF $p(\epsilon)$ as well, since $\mathbf{R}_\epsilon^T = \exp((-\epsilon)^\wedge)$.

Based on the observation (7), the proposed estimator will estimate the position vector \mathbf{r} and the rotation matrix \mathbf{R} from the incoming light in the optical receiver, assuming $\tilde{\mathbf{R}}$ and $p(\mathbf{R}_\epsilon)$ are known.

III. RSS-BASED HYBRID ML/MAP ESTIMATION

In this section, we propose the HyMM estimator, which takes into account the prior information on the orientation $p(\mathbf{R}|\tilde{\mathbf{R}})$, for the receiver with a PD array, and compare it with two state-of-the-art estimators.

In our previous work [20], we introduced a SPO algorithm that estimates the position and orientation of the receiver using the received light signal only, i.e. no prior information is available on the orientation. In this paper, we assume prior information is available on the orientation, as described

in the previous section. Prior information on a parameter to be estimated can be included by considering the MAP principle, using the joint PDF $p(\mathbf{y}, \Theta)$, where $\Theta = \{\mathbf{r}, \mathbf{R}\}$ consisting of the position vector \mathbf{r} and the rotation matrix \mathbf{R} , is the parameter set to be estimated. However, only for the orientation \mathbf{R} , prior information is available, implying the MAP principle cannot be applied on the position estimation. Another approach to include the orientation uncertainty is to consider the orientation as a nuisance parameter and use the ML principle to estimate the position only, using the likelihood function $p(\mathbf{y}|\tilde{\mathbf{R}}; \mathbf{r}) = \int_{\mathbf{R}} p(\mathbf{y}, \mathbf{R}|\tilde{\mathbf{R}}; \mathbf{r}) d\mathbf{R}$. However, although the distribution of ϵ is Gaussian, the rotation matrix \mathbf{R}_ϵ is not Gaussian distributed, as it is a non-linear transformation of ϵ . As a consequence, $\int_{\mathbf{R}} p(\mathbf{y}, \mathbf{R}|\tilde{\mathbf{R}}; \mathbf{r}) d\mathbf{R}$ becomes analytically intractable. To overcome the issues in the above mentioned approaches, we use as alternative the HyMM principle [26], [27], [39] to jointly estimate the position and orientation of the receiver. In a hybrid ML/MAP estimator, the parameter set to be estimated is a combination of parameters with and without prior information. In this paper, the hybrid parameter set Θ is defined as $\Theta = \{\mathbf{r}, \mathbf{R}\}$, where \mathbf{r} is the position vector without prior information and \mathbf{R} is the rotation matrix with prior information. The HyMM estimator then jointly estimates \mathbf{r} and \mathbf{R} based on the joint PDF:

$$\begin{aligned} p(\mathbf{y}, \mathbf{R}|\tilde{\mathbf{R}}; \mathbf{r}) &= p(\mathbf{y}|\mathbf{R}; \mathbf{r})p(\mathbf{R}|\tilde{\mathbf{R}}) \\ &= p(\mathbf{y}|\Theta)p(\epsilon) |\det(\nabla_{\mathbf{R}}\epsilon)| \end{aligned} \quad (9)$$

where $p(\mathbf{y}|\Theta)$ is Gaussian distributed with $\mathbf{y}|\Theta \sim \mathcal{N}(\mathbf{h}(\Theta), \Sigma_w)$, and the conditional PDF $p(\mathbf{R}|\tilde{\mathbf{R}})$ giving the prior information about \mathbf{R} is specified by $p(\mathbf{R}_\epsilon^T)$. In (9), the distribution of \mathbf{R}_ϵ^T is represented in terms of ϵ , which is Gaussian, using the relation $\epsilon = \log(\mathbf{R}_\epsilon)^V \sim \mathcal{N}(\mathbf{0}, \Sigma_\epsilon)$, the last factor in the last equality of (9) comes from the change of variables, and the expressions of the Jacobian $\nabla_{\mathbf{R}}\epsilon$ and $|\det(\nabla_{\mathbf{R}}\epsilon)|$ are given in Appendix B.

Based on (9), the HyMM principle yields the estimate $\hat{\Theta} = \{\hat{\mathbf{r}}, \hat{\mathbf{R}}_\epsilon\}$ that maximizes the hybrid log-likelihood function:

$$\hat{\Theta} = \arg \max_{\Theta} \mathcal{L}_H(\Theta; \mathbf{y}, \tilde{\mathbf{R}}), \quad (10)$$

and

$$\begin{aligned} \mathcal{L}_H(\Theta; \mathbf{y}, \tilde{\mathbf{R}}) &= \ln p(\mathbf{y}|\Theta) + \ln p(\epsilon) + \ln |\det(\nabla_{\mathbf{R}}\epsilon)| \\ &\approx \text{const} - \frac{1}{2} \|\mathbf{y} - \mathbf{h}\|_{\Sigma_w}^2 - \frac{1}{2} \|\epsilon\|_{\Sigma_\epsilon}^2. \end{aligned} \quad (11)$$

In (11), we neglected the effect of the determinant (36), because in most practical situations ϵ is small so that $|\det(\nabla_{\mathbf{R}}\epsilon)|$ approaches 1 (see Appendix B), and neglecting this factor will result in an estimator with lower computational complexity. Next, we introduce two expanded vectors,

$$\check{\mathbf{y}} = [\mathbf{y}^T \mathbf{0}_{1 \times 3}]^T \in \mathbb{R}^{(N_L N_P + 3) \times 1}, \quad (12)$$

$$\check{\mathbf{h}} = [\mathbf{h}^T \sigma_w \epsilon^T \Sigma_\epsilon^{-\frac{1}{2}}]^T \in \mathbb{R}^{(N_L N_P + 3) \times 1}, \quad (13)$$

with $\Sigma_\epsilon^{-\frac{1}{2}}$ the matrix square root of Σ_ϵ^{-1} , and combine the last two terms in (11) to obtain

$$\mathcal{L}_H(\Theta; \mathbf{y}, \tilde{\mathbf{R}}) = \text{const} - \frac{1}{2\sigma_w^2} (\check{\mathbf{y}} - \check{\mathbf{h}})^T (\check{\mathbf{y}} - \check{\mathbf{h}}). \quad (14)$$

In this way, (10) is turned into a constrained non-linear least squares (NLS) problem given by

$$\begin{aligned} \hat{\Theta} &= \arg \min_{\Theta} (\|\check{\mathbf{y}} - \check{\mathbf{h}}\|^2) \\ \text{s.t. } &\mathbf{R}^T \mathbf{R} = \mathbf{R} \mathbf{R}^T = \mathbf{I}_3, \\ &\det(\mathbf{R}) = +1, \end{aligned} \quad (15)$$

where the constraints impose that \mathbf{R} must be a member of $SO(3)$. However, this constrained optimization problem has no closed-form solution and is non-convex, implying we need to resort to constrained non-linear optimization algorithms, which are complex, time consuming and non-robust. As an alternative, since $SO(3)$ is an embedded submanifold of $\mathbb{R}^{3 \times 3}$, we can estimate \mathbf{R} using the Gauss-Newton algorithm on the manifold $SO(3)$ [20]. In this algorithm, we iteratively update the estimates of $\Theta = \{\mathbf{r}, \mathbf{R}\}$ using

$$\mathbf{r}^{t+1} = \mathbf{r}^t + \Delta_{\mathbf{r}} \quad \text{and} \quad \mathbf{R}^{t+1} = \exp((\Delta_{\mathbf{R}})^\wedge) \mathbf{R}^t \quad (16)$$

where the incremental step $\Delta_{\Theta} = [\Delta_{\mathbf{r}}^T, \Delta_{\mathbf{R}}^T]^T$ is calculated by

$$\Delta_{\Theta} = -\eta (\nabla_{\Theta} \check{\mathbf{h}})^\dagger (\check{\mathbf{h}} - \check{\mathbf{y}}), \quad (17)$$

with η the step size, $(\cdot)^\dagger$ the Moore-Penrose pseudoinverse, and

$$\nabla_{\Theta} \check{\mathbf{h}} = \begin{bmatrix} \nabla_{\Theta} \mathbf{h} \\ \mathbf{0}_{3 \times 3} & \sigma_w \Sigma_\epsilon^{-\frac{1}{2}} \nabla_{\mathbf{R}} \epsilon \end{bmatrix} \in \mathbb{R}^{(N_L N_P + 3) \times 6} \quad (18)$$

the expanded Jacobian matrix with respect to Θ . The Jacobian matrix of \mathbf{h} with respect to Θ is the $N_L N_P \times 6$ matrix $\nabla_{\Theta} \mathbf{h} = [\nabla_{\Theta} \mathbf{h}_1, \dots, \nabla_{\Theta} \mathbf{h}_{N_P}]^T$ with $\nabla_{\Theta} \mathbf{h}_j = R_{p,j} [P_{t,1} \nabla_{\Theta} h_{1,j}, \dots, P_{t,N_L} \nabla_{\Theta} h_{N_L,j}]^T$, where the expression for $\nabla_{\Theta} h_{i,j}$ can be found in Appendix B.

In this paper, we compare the performance of the proposed HyMM estimator with the performance of the SPO, MML and AP1st estimators. To better understand the results for these three state-of-the-art algorithms, we briefly review the objective functions used by these algorithms. In the SPO estimator, the algorithm fully distrusts the available orientation estimate $\tilde{\mathbf{R}}$ from the external device and assumes that no reliable information about $p(\mathbf{R}_\epsilon)$ is available, implying it has to estimate Θ from the observed vector \mathbf{y} only. Consequently, the log-likelihood equals $\mathcal{L}(\Theta; \mathbf{y}) = \ln p(\mathbf{y}|\Theta)$ [20]. In the MML estimator, the algorithm fully trusts the estimate of the orientation $\tilde{\mathbf{R}}$ and neglects the orientation uncertainty, i.e. the estimator misspecifies $\mathbf{R}_\epsilon = \mathbf{I}_3$ as a constant, implying the distribution of the vector of observed light signals is modeled as $\mathbf{y}|\tilde{\mathbf{R}} \sim \mathcal{N}(\mathbf{h}(\mathbf{r}, \tilde{\mathbf{R}}), \Sigma_w)$. From the resulting misspecified distribution $p_m(\mathbf{y}|\mathbf{r}; \tilde{\mathbf{R}})$, the MML estimator obtains the estimate through the maximization of the likelihood function $\mathcal{L}_M(\mathbf{r}; \mathbf{y}) = \ln p_m(\mathbf{y}|\mathbf{r}; \tilde{\mathbf{R}})$. Finally, the AP1st algorithm approximates the likelihood function of \mathbf{r} with the PDF $p_a(\mathbf{y}|\mathbf{r}; \tilde{\mathbf{R}})$ corresponding to $\mathbf{y}|\mathbf{r} \sim \mathcal{N}(\mathbf{h}(\mathbf{r}, \tilde{\mathbf{R}}), \Sigma_y)$, where $\Sigma_y = (\nabla_{\mathbf{R}}|_{\tilde{\mathbf{R}}} \mathbf{h}) \Sigma_\epsilon (\nabla_{\mathbf{R}}|_{\tilde{\mathbf{R}}} \mathbf{h})^T + \Sigma_w$ with the Jacobian matrix $\nabla_{\mathbf{R}}|_{\tilde{\mathbf{R}}} \mathbf{h}$ of \mathbf{h} with respect to \mathbf{R} evaluated at $\tilde{\mathbf{R}}$. Based on the approximated distribution $p_a(\mathbf{y}|\mathbf{r}; \tilde{\mathbf{R}})$, the AP1st

algorithm obtains the estimate through the maximization of the likelihood function $\mathcal{L}_A(\mathbf{r}; \mathbf{y}) = \ln p_a(\mathbf{y}|\mathbf{r}; \tilde{\mathbf{R}})$ [25]. Notice that the AP1st algorithm does not estimate the orientation, i.e., it is a positioning algorithm.

Besides the performance of the algorithms, which will be discussed in Section V, we are also interested in their complexity. All algorithms except AP1st can be converted into a NLS problem, which can be solved with the Gauss-Newton method. In the Gauss-Newton method, the complexity during each iteration is dominated by the computation of the Moore-Penrose pseudoinverse. As a consequence, the HyMM, SPO and MML algorithm, respectively, have a complexity of $\mathcal{O}(6(N_L N_P + 3)^2)$, $\mathcal{O}(6(N_L N_P)^2)$ and $\mathcal{O}(3(N_L N_P)^2)$ flops per iteration. On the other hand, the complexity of the AP1st algorithm is dominated by the matrix inversion of $\Sigma_{\mathbf{y}}$ required to obtain the gradient in each inner iteration. Therefore, the AP1st algorithm has a complexity of $\mathcal{O}((N_L N_P)^3)$ flops per iteration. Hence, it is clear that the complexity of the HyMM algorithm is lower than that of the AP1st algorithm but roughly equivalent to the complexity of the other algorithms.

IV. THEORETICAL LOWER BOUND

In the numerical results section, we will use the mean squared error (MSE) to compare the performance of the proposed HyMM estimator with the performance of the SPO estimator and MML estimator. As no closed-form solution is available for the estimators, we will determine the performance through simulations. To obtain insight into the optimality of the proposed estimator, in this section, we derive the hybrid Cramér-Rao lower bound (HCRB), which is the theoretical lower bound on the MSE for the HyMM estimator.

Using this HCRB, we can evaluate the estimation errors on the position, which is expressed by the Euclidean distance between $\hat{\mathbf{r}}$ and \mathbf{r} , i.e. $\mathbf{r}_e = \hat{\mathbf{r}} - \mathbf{r}$, and on the axis-angle vector between $\hat{\mathbf{R}}$ and \mathbf{R} , i.e. $\mathbf{u}_e = \log(\hat{\mathbf{R}}\mathbf{R}^T)^\vee$ [20]. In order to obtain the HCRB, first we need to calculate the hybrid information matrix (HIM) \mathbf{J}_H , which is given by [26]

$$\begin{aligned} \mathbf{J}_H &= -E_{\mathbf{y}, \mathbf{R}|\tilde{\mathbf{R}}, \mathbf{r}} \left\{ \nabla_{\Theta} \nabla_{\Theta}^T \ln p(\mathbf{y}, \mathbf{R}|\tilde{\mathbf{R}}, \mathbf{r}) \right\} \\ &= \mathbf{J}_D + \mathbf{J}_P. \end{aligned} \quad (19)$$

where $E_{\mathbf{x}}\{f\}$ is the expectation of f with respect to the PDF of \mathbf{x} , and $\mathbf{J}_D = -E_{\mathbf{y}, \mathbf{R}|\tilde{\mathbf{R}}, \mathbf{r}} \left\{ \nabla_{\Theta} \nabla_{\Theta}^T \ln p(\mathbf{y}|\Theta) \right\}$ represents the contribution of the data (observed light signal), $\mathbf{J}_P = -E_{\mathbf{R}|\tilde{\mathbf{R}}} \left\{ \nabla_{\Theta} \nabla_{\Theta}^T \ln p(\mathbf{R}|\tilde{\mathbf{R}}) \right\}$ represents the contribution of the prior information on the orientation:

$$\mathbf{J}_D = E_{\mathbf{R}|\tilde{\mathbf{R}}} \{ \mathbf{J}_F(\Theta) \}, \quad (20)$$

$$\mathbf{J}_P = \begin{bmatrix} \mathbf{0} & \mathbf{0} \\ \mathbf{0} & \mathbf{J}_{\mathbf{R}} \end{bmatrix}. \quad (21)$$

Since $\mathbf{y}|\Theta$ is multivariate Gaussian with its covariance being independent of Θ , the associated Fisher information matrix (FIM) $\mathbf{J}_F(\Theta)$, i.e., the operand of the expectation in (20), can be calculated as [40]:

$$\mathbf{J}_F(\Theta) = \frac{1}{\sigma_w^2} (\nabla_{\Theta} \mathbf{h})^T (\nabla_{\Theta} \mathbf{h}). \quad (22)$$

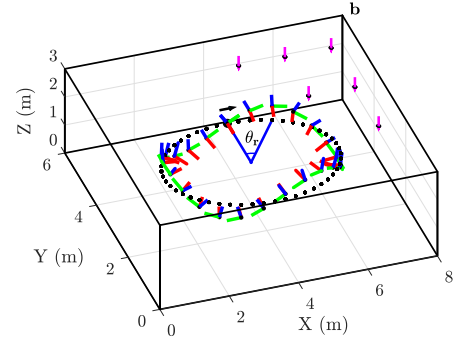


Fig. 3. Simulation setup. The three orthonormal vectors in three different colors (the red, green and blue vector represent the x -axis, y -axis and z -axis, respectively) at each sample on the path represent the frame of the receiver. The pink arrows represent the LEDs (only a fraction of them are shown) on the ceiling. θ_r indicates the traveled angle along the dotted ellipse in the XY plane.

Further, the non-zero submatrix of (21) equals $\mathbf{J}_{\mathbf{R}} = E_{\mathbf{R}|\tilde{\mathbf{R}}} \left\{ (\nabla_{\mathbf{R}} \ln p(\mathbf{R}|\tilde{\mathbf{R}}))^T (\nabla_{\mathbf{R}} \ln p(\mathbf{R}|\tilde{\mathbf{R}})) \right\}$, with $\nabla_{\mathbf{R}} \ln p(\mathbf{R}|\tilde{\mathbf{R}})$ given in Appendix B. Due to the complexity of $p(\mathbf{R}|\tilde{\mathbf{R}})$, the expectations for computing (20) and (21) are analytically intractable. Therefore, we calculate them numerically via Monte Carlo integration [41]:

$$\mathbf{J}_D \approx \frac{1}{N_M} \sum_{n=1}^{N_M} \mathbf{J}_F(\{\mathbf{r}, \mathbf{R}_n\}), \quad (23)$$

and

$$\mathbf{J}_{\mathbf{R}} \approx \frac{1}{N_M} \sum_{n=1}^{N_M} (\nabla_{\mathbf{R}} \ln p(\mathbf{R}|\tilde{\mathbf{R}}))^T (\nabla_{\mathbf{R}} \ln p(\mathbf{R}|\tilde{\mathbf{R}})) \Big|_{\mathbf{R}_n}, \quad (24)$$

where \mathbf{R}_n , $n = 1, \dots, N_M$ are i.i.d. samples generated from $p(\mathbf{R}|\tilde{\mathbf{R}})$. To get the lower bound on the error covariance matrices of \mathbf{r}_e and \mathbf{u}_e , we first rewrite the HIM \mathbf{J}_H as a partitioned matrix,

$$\mathbf{J}_H = \begin{bmatrix} \mathbf{J}_{H,r,r} & \mathbf{J}_{H,r,\mathbf{R}} \\ \mathbf{J}_{H,\mathbf{R},r} & \mathbf{J}_{H,\mathbf{R},\mathbf{R}} \end{bmatrix}. \quad (25)$$

Consequently,

$$E\{\mathbf{r}_e \mathbf{r}_e^T\} \succeq \left[\mathbf{J}_{H,r,r} - \mathbf{J}_{H,r,\mathbf{R}} \mathbf{J}_{H,\mathbf{R},\mathbf{R}}^{-1} \mathbf{J}_{H,\mathbf{R},r} \right]^{-1} \quad (26)$$

and

$$E\{\mathbf{u}_e \mathbf{u}_e^T\} \succeq \left[\mathbf{J}_{H,\mathbf{R},\mathbf{R}} - \mathbf{J}_{H,\mathbf{R},r} \mathbf{J}_{H,r,r}^{-1} \mathbf{J}_{H,r,\mathbf{R}} \right]^{-1}. \quad (27)$$

V. NUMERICAL RESULTS

In the evaluation of the hybrid ML/MAP estimator and the theoretical lower bound in the presence of prior information on the orientation through computer simulations, we consider an $8 \text{ m} \times 6 \text{ m} \times 3 \text{ m}$ area in which $N_L = 24$ LEDs are mounted at the ceiling of the area, as shown in Fig. 3. We define the boundary vector $\mathbf{b} = [8, 6, 3]^T$, the number of LED columns in the X direction $N_{L,X} = 6$ and Y direction $N_{L,Y} = 4$, and the positions of the LEDs are given by $\left[\frac{\mathbf{b}_1(2i-1)}{2N_{L,X}}, \frac{\mathbf{b}_2(2j-1)}{2N_{L,Y}}, \mathbf{b}_3 \right]^T$, with $i \in \{1, \dots, N_{L,X}\}$ and

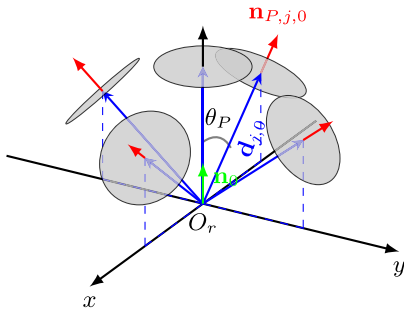


Fig. 4. Angular diversity receiver with $N_{P,s} = 4$.

$j \in \{1, \dots, N_{L,Y}\}$, where $[\mathbf{b}]_i$ denotes the i^{th} component of \mathbf{b} . In the following, it is assumed that all LEDs have a same transmit power, a normal $\mathbf{n}_i = [0, 0, -1]^T$ (pointing downwards), and a Lambertian order $\gamma = 1$, $i \in \{1, \dots, N_L\}$ implying a half-intensity beam angle of $\pi/3$, and a FOV angle $\phi_{FOV} = \pi/2$.

To evaluate the performance of the proposed estimators, we consider a path with an elliptical pattern in the XY plane and a sinusoidal pattern in the Z direction, as shown in Fig. 3. The semi-major axis and the semi-minor axis of the ellipse are 2.5 m and 1.5 m, respectively, and the amplitude of the sinusoidal pattern is 0.5 m. The ellipse (the dotted ellipse) is centered at $[4.0, 3.0, 1.5]^T$ m, i.e. the center of the considered area. Starting at the coordinates $[4.0, 4.5, 1.5]^T$ m (the black arrow), the path oscillates sinusoidally in the Z direction and completes the path in three periods. The receiver follows the path clockwise, and at each sample point the orientation of the receiver is chosen such that the frame of the receiver is tangent to the path, more specifically, the rotation matrix \mathbf{R} representing the orientation of the receiver is given by $\mathbf{R} = [\mathbf{n}_{R,x}, \mathbf{n}_{R,y}, \mathbf{n}_{R,z}]$, where $\mathbf{n}_{R,y}$ is the unit tangent vector of the path at the sample point, $\mathbf{n}_{R,x}$ the unit vector in the XY plane satisfying $\mathbf{n}_{R,x}^T \mathbf{n}_{R,y} = 0$ and $\mathbf{n}_{R,z} = \mathbf{n}_{R,x} \times \mathbf{n}_{R,y}$, with \times the vector product and $[\mathbf{n}_{R,z}]_3 > 0$. The frame of the receiver (the column vectors of \mathbf{R}) at each sample on the path is illustrated in Fig. 3 by three orthonormal vectors in three different colors. We use the parameter θ_r to specify the sample point, where θ_r is the traveled angle along the ellipse in the XY plane.

We consider the called angular diversity receiver from [42]–[44]. Before situating the receiver in the system frame with its orientation \mathbf{R} and position \mathbf{r} , we first describe the receiver layout in the receiver frame. The receiver consists of $N_P = 5$ PDs, where $N_{P,s} = 4$ PDs are placed symmetrically around the center of the receiver, and are tilted away from the center of the receiver by $\theta_P = \pi/4$, as shown in Fig. 4. The normal of the j^{th} PD, $j \in \{1, \dots, N_{P,s}\}$ is given by $\mathbf{n}_{P,j,0} = \exp((\theta_P \mathbf{z}_{P,j})^\wedge) \mathbf{n}_0$, where $\mathbf{z}_{P,j} = [\cos(j2\pi/N_{P,s}), \sin(j2\pi/N_{P,s}), 0]^T$ and the reference vector $\mathbf{n}_0 = [0, 0, 1]^T$. The last PD is placed right above the center of the receiver and thus has normal \mathbf{n}_0 . The relative distance vector $\mathbf{d}_{j,0}$ that specifies the position of the j^{th} PD, $j \in \{1, \dots, N_P\}$, to the center of the receiver is given by $\mathbf{d}_{j,0} = d_j \mathbf{n}_{P,j,0}$, with $d_j = 0.02$ m. All PDs are assumed to have a FOV angle $\theta_{FOV} = 4\pi/9$, an average

responsivity $R_p = 0.3$ A/W and an area $A_R = \pi r_P^2$ with radius $r_P = 1 \times 10^{-3}$ m. In the following, we assume the receiver is subject to an orientation uncertainty with covariance matrix $\Sigma_\epsilon = \sigma_\epsilon^2 \mathbf{I}_{3 \times 3}$. Unless specified otherwise, we assume $\sigma_\epsilon^2 = 1 \times 10^{-2}$ rad². Finally, the SNR² is defined as $\text{SNR} \triangleq \left(\frac{(\gamma+1)A_R P_t R_p}{2\pi\sigma_w} \right)^2$. We assume the shot noise has power spectral density $N_0 = 5.25 \times 10^{-23}$ A²/Hz, which corresponds to a background spectral irradiance $p_n = 5.8 \times 10^{-6}$ W/(cm²·nm) with a visible light bandwidth $\Delta\lambda = 360$ nm [12], and assume an amplifier noise density $I_a = 5 \times 10^{-12}$ A/ $\sqrt{\text{Hz}}$ [45] and an electrical bandwidth $B = 1$ MHz [46], then the noise variance σ_w^2 can be calculated as $\sigma_w^2 = (N_0 + I_a^2)B$ [45]. Considering an optical transmit power $P_t = 1$ W, this results in an SNR = 34.5 dB. In our simulations, we will use the range SNR $\in [0, 70]$ dB to take into account variations of the system parameters.

As the algorithms considered in this paper require an iterative procedure, they need an initial estimate of the position and the orientation. For the HyMM, MML and AP1st estimators, the initial estimate of the orientation comes from the external device, while for the position, we take as initial point the center of the area, i.e. $\hat{\Theta}^0 = \{\mathbf{b}/2, \tilde{\mathbf{R}}\}$. Similarly, the SPO algorithm considers as initial estimate of the position the center of the area. However, the SPO algorithm has no prior knowledge on the orientation. Therefore, we assume we have a coarse orientation estimator that estimates the orientation from the optical signal as e.g. described in [20]. To have a fair comparison with the HyMM and MML estimators, we assume this coarse estimator delivers a coarse estimate of the orientation that is Gaussian distributed around the true value of the orientation with variance $\sigma_0^2 = \sigma_\epsilon^2$, i.e., the SPO algorithm is initialized with $\hat{\Theta}^0 = \{\mathbf{b}/2, \hat{\mathbf{R}}^0\}$ with $\log(\hat{\mathbf{R}}^0 \mathbf{R}^T)^\vee \sim \mathcal{N}(\mathbf{0}, \sigma_0^2 \mathbf{I}_3)$.

A. Performance of the Hybrid ML/MAP Estimator

In Fig. 5, we show the root of the mean squared error (RMSE) of the position and orientation estimates of the proposed HyMM estimator as a function of the position θ_r of the receiver in the elliptical path for SNR = 15 dB and SNR = 35 dB, respectively, and compare the resulting RMSE with the RMSE of the simultaneous position and orientation estimator (SPO), the misspecified maximum likelihood estimator (MML) and the first-order-approximation-based positioning algorithm (AP1st). Further, we show in the figure the root of the theoretical lower bound (HMMLB) from Section IV, and the root of the theoretical lower bounds for the SPO and MML estimators,³ denoted by SPOB and MMLB,

²Since the received SNR depends on the receiver's position and orientation, fixing the received SNR in the simulation will set a confinement on the parameter space of receiver's position and orientation. To solve this complication, we instead use the SNR defined above, which discards the position- and orientation-related dependency in the received power. Taking into account the definition of the channel gain $h_{i,j}$ (5), it follows that the received SNR is proportional to the above defined SNR by a factor $\left(\frac{2\pi h_{i,j}}{(\gamma+1)A_R} \right)^2$. In other words, the used SNR is equal to the received SNR for a PD, right below a LED and pointing to that LED, i.e. $\theta_{i,j} = \phi_{i,j} = 0$ rad, at a distance of $v_{i,j} = 1$ m.

³The theoretical lower bound for the SPO estimator is found in [20], while the bound for the MML estimator is discussed in Appendix A.

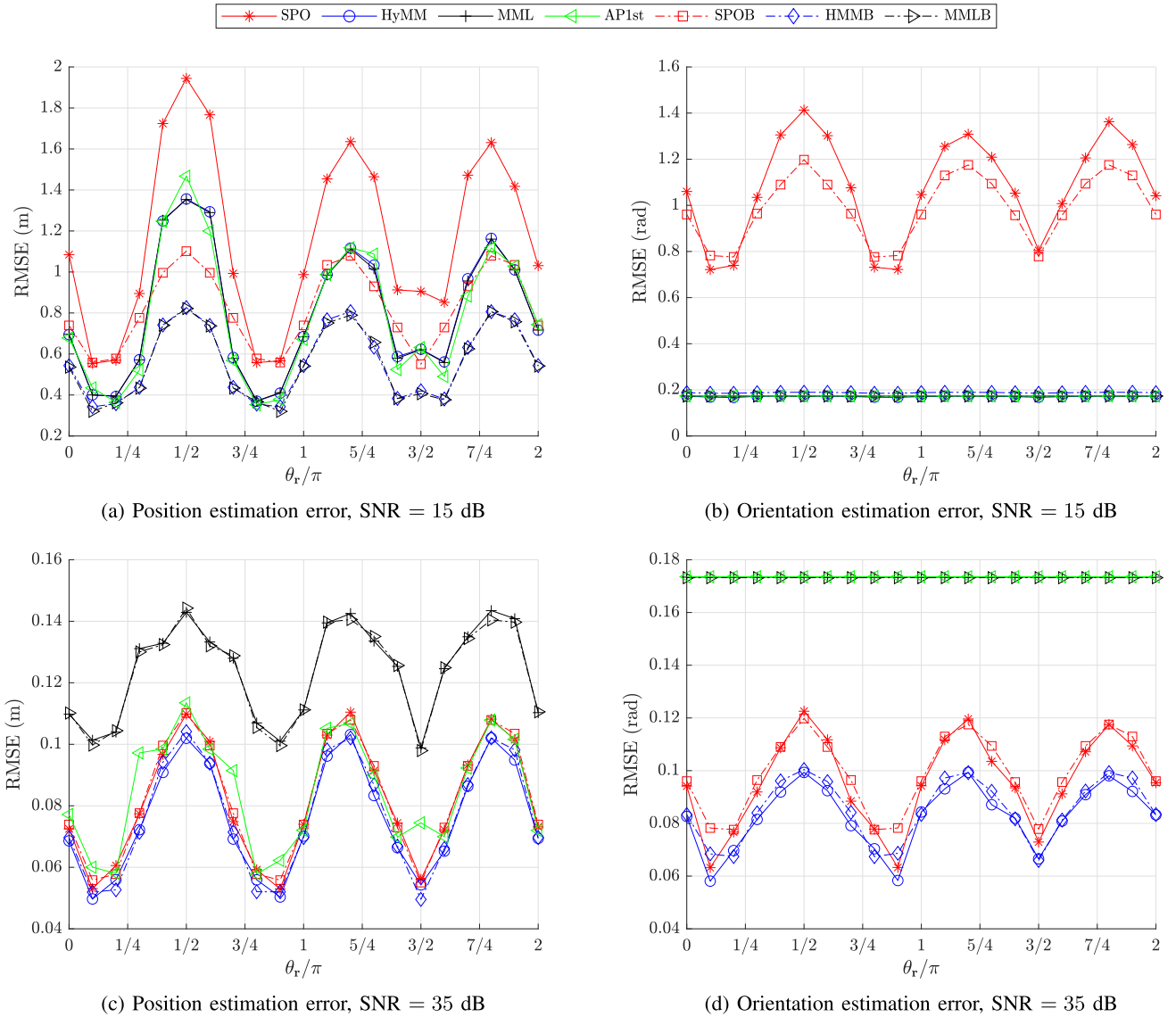


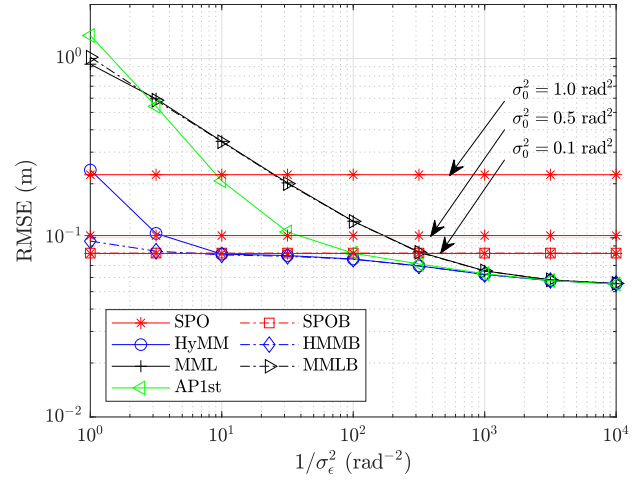
Fig. 5. RMSE of the estimator as a function of the traveled angle θ_r along the elliptical path for $\sigma_\epsilon^2 = 1 \times 10^{-2} \text{ rad}^2$.

respectively. Let us first take a closer look at the behavior of the estimators and bounds as function of the traveled angle θ_r along the elliptical path. The path we consider has a sinusoidal pattern in the Z direction, implying the distance between the receiver and the LED is relatively larger in the valleys of the path. At the same time, the path has an elliptical pattern in the XY plane. Taking into account the uniform distribution of the LEDs in the area, it is clear that the average distance between the LEDs and the receiver is the largest in the vertices. Hence, the largest average distance will occur at the vertex lying in a valley, i.e. for $\theta_r = \pi/2$. Because the channel gain is inversely proportional to the distance between the receiver and the LEDs, a higher RMSE is expected at those points in the path that have a larger (average) distance between the receiver and the LEDs. This can be observed in Fig. 5, where the RMSE performance along the path shows a sinusoid-like pattern with three peaks and valleys, corresponding to the valleys and peaks in the path. As expected, the largest RMSE is obtained around

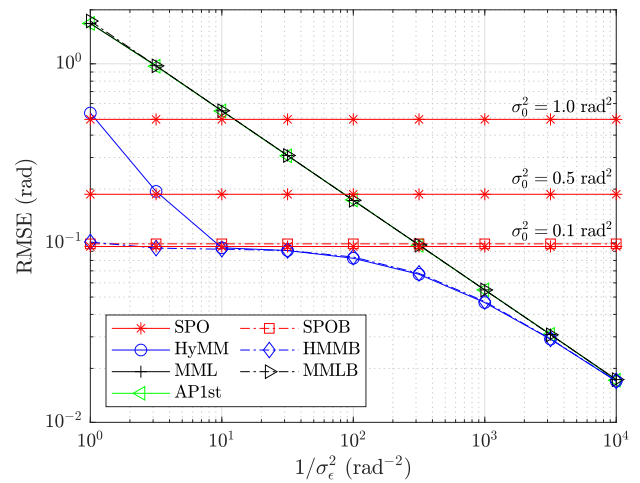
$\theta_r = \pi/2$, which corresponds to the vertex in the valley. Next, we look at the performance of position estimation, as shown in Figs. 5a and 5c. As can be observed, for SNR = 15 dB, the MML, AP1st and HyMM algorithms have similar positioning performance, while the SPO algorithm has a noticeable larger RMSE. On the other hand, when SNR = 35 dB, the HyMM, AP1st and SPO algorithms have similar performance, and the MML algorithm has a noticeably larger RMSE. This can be explained as follows. On the one hand, when the SNR is low, it will be hard to extract reliable information about the position and orientation from the optical signal. A relatively accurate external estimate of the orientation, as available in the HyMM, MML and AP1st estimators, can help to improve the position estimate. On the other hand, for larger SNR, reliable information about the position and orientation can be extracted from the optical signal, implying the performance will be less determined by the presence of a noisy prior estimate of the orientation. As the MML algorithm neither

takes into account the orientation uncertainty and nor updates the orientation estimate using the optical signal, the effect of the misspecification of the orientation on the position estimate cannot be completely compensated by the reliable optical signal. In contrast, the SPO algorithm and HyMM algorithm estimate the orientation both from the reliable optical signal, while the AP1st algorithm takes into account the orientation uncertainty. This explains the similar positioning performance of the three latter algorithms. Comparing the RMSE performance of the algorithms with their respective lower bounds, we see for SNR = 15 dB a gap between the RMSE and the lower bound, while for SNR = 35 dB, the RMSE is close to the lower bound. The reason for this is the asymptotic tightness of the CRB, i.e. the lower bound is tight when the SNR or the number of observations is sufficiently large. Finally, we look at the performance of the orientation estimation, shown in Figs. 5b and 5d. As the performance of the external orientation estimator is independent of the position of the receiver and the optical signal, the RMSE of the MML and AP1st estimators will be constant over the whole path and independent of the SNR of the optical signal, i.e. the level of the RMSEs of MML and AP1st are the same for both Figs. 5b and 5d. Similarly as for the position estimate, the RMSE of the HyMM estimator is similar to that of the MML estimator for SNR = 15 dB and similar to that of the SPO estimator for SNR = 35 dB. For low SNR, the SPO estimator is not able to extract a reliable orientation estimate from the optical signal, yielding a worse RMSE than the others', while for larger SNR, the reliable optical signal allows the HyMM and SPO estimator to obtain a more accurate orientation estimate than available with the external device, implying the MML and AP1st algorithms will have worse performance. Again, the explanation can be found in the reliability of the optical signal and the relative effect of the noisy prior estimate of the orientation at low and high SNR, similarly as for the position estimate. Also for the orientation estimate, the lower bound is tight for sufficiently high SNR. As a conclusion, the proposed HyMM estimator combines the best of both worlds: for low SNR as well as for high SNR, the RMSE of the proposed HyMM estimator for both the position and orientation is at least as good or better than for the state-of-the-art algorithms, and operates close to optimal.

Next, we look at the effect of the variance σ_ϵ^2 of the orientation uncertainty. Fig. 6 shows the RMSE, averaged over the entire path, as a function of $1/\sigma_\epsilon^2$ for SNR = 35 dB. As the SPO algorithm does not use an orientation estimate from an external device, the performance of the SPO estimator is independent of σ_ϵ^2 , in contrast to the performance of the other estimators. The SPO performance only depends on the accuracy of the coarse orientation estimate, i.e., σ_0^2 . As can be observed in the figure, for large σ_0^2 , the SPO algorithm is not able to reach the theoretical lower bound. Due to the inaccuracy of the coarse estimate, the iterative algorithm in the SPO estimator is not able to converge properly to the correct position and orientation. From our simulations, we observed that the SPO algorithm converges correctly for a value of σ_0^2 up to 0.1 rad². Let us now look closer at the dependency of the other estimators on the variance σ_ϵ^2 . First note that the MML and AP1st estimators do not estimate the orientation based on



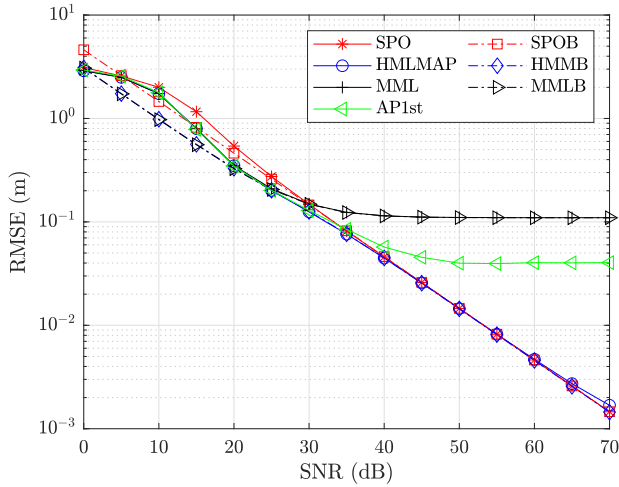
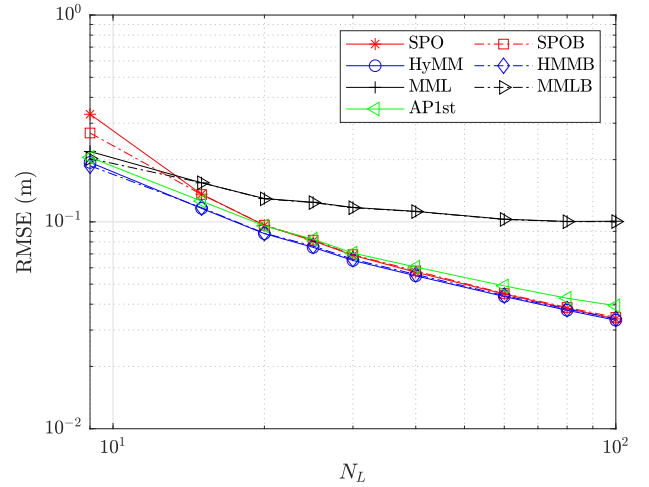
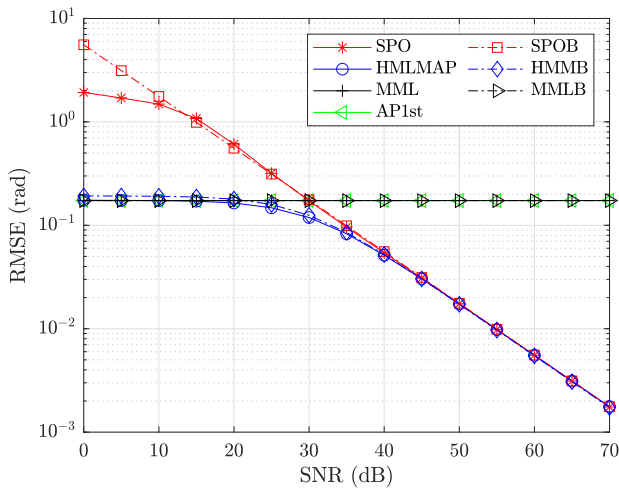
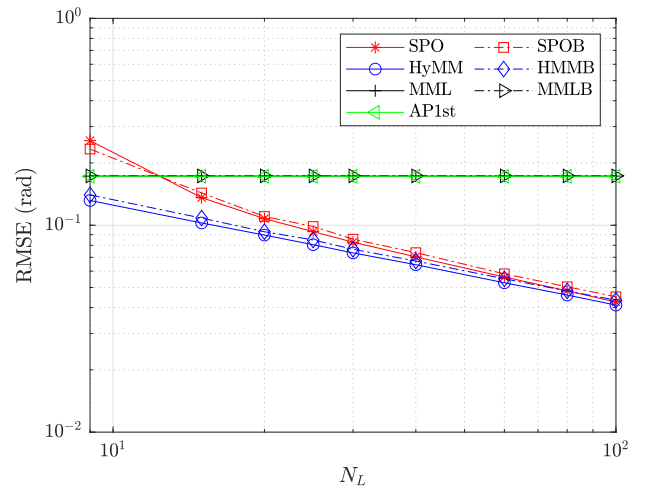
(a) Position estimation error



(b) Orientation estimation error

 Fig. 6. RMSE versus $1/\sigma_\epsilon^2$ for SNR = 35 dB.

the optical signal. Hence, the RMSE of the orientation estimate is determined by the variance σ_ϵ^2 of the external orientation estimate. When the variance σ_ϵ^2 is large, i.e. $1/\sigma_\epsilon^2$ is small, the external orientation estimate is inaccurate. This will strongly reduce the positioning performance of the MML estimator, while the AP1st achieves a better positioning performance due to taking into account the orientation uncertainty. However, the inaccuracy of the first-order approximation leads the AP1st to perform worse than HyMM, and it even underperforms MML when σ_ϵ^2 becomes too large, implying the approximation becomes inaccurate and results in an incorrect position estimate. Comparing the lower bounds on the performance of the SPO and HyMM algorithm, we observe that the theoretical performance of both estimators is similar. This could be expected as due to the unreliable external orientation estimate, the performance of the HyMM estimator will be determined by the quality of the optical signal, similarly as for the SPO algorithm. On the other hand, when the variance σ_ϵ^2 is small, i.e. $1/\sigma_\epsilon^2$ is large, the external orientation estimate is accurate. In this case, the performance of the orientation estimate

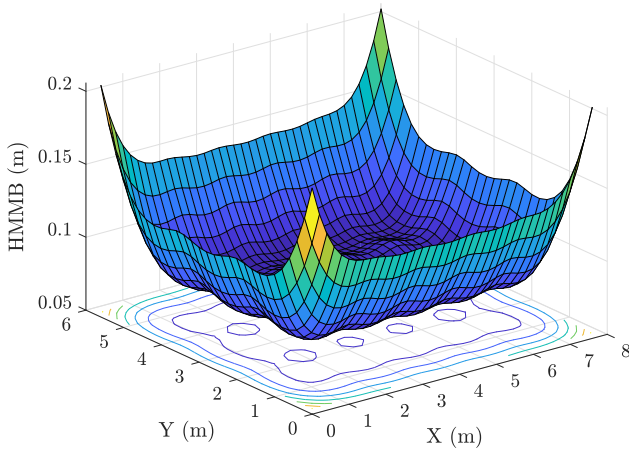
(a) Position error versus SNR, $N_L = 24$ (b) Position error versus N_L , SNR = 35 dB(c) Orientation error versus SNR, $N_L = 24$ (d) Orientation error versus N_L , SNR = 35 dBFig. 7. RMSE of position and orientation estimates versus SNR and N_L .

is mainly determined by the external estimator, implying the HyMM, MML and AP1st estimators will have similar performance. The SPO algorithm is not able to achieve the same accuracy for the orientation based on the information contained in the optical signal, implying the performance of the SPO algorithm is degraded compared to other.

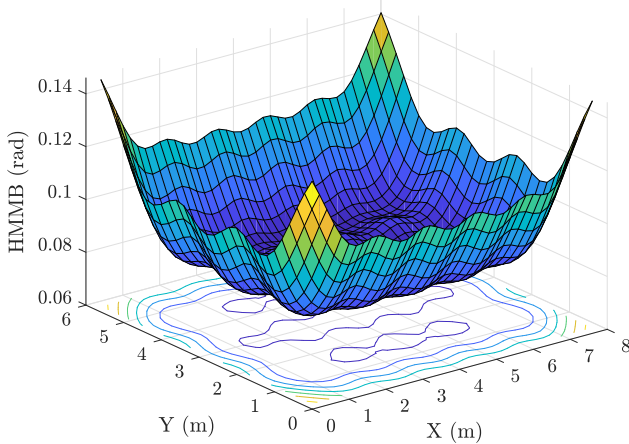
B. Asymptotic Tightness

In this section, we show that the proposed estimator is asymptotically tight with its lower bound for sufficiently large SNR or number of LEDs. In our simulations, we use the same path for the receiver as shown in Fig. 3, and the RMSE and associated root of the theoretical bound are averaged over the path. First, in Figs. 7a and 7c, we show the averaged RMSE for the position and orientation, respectively, as a function of the SNR for $N_L = 24$ LEDs. The results show that the proposed HyMM estimator is indeed asymptotically tight for large SNR. A similar asymptotic tightness is obtained with the SPO and MML estimators to their respective lower bounds.

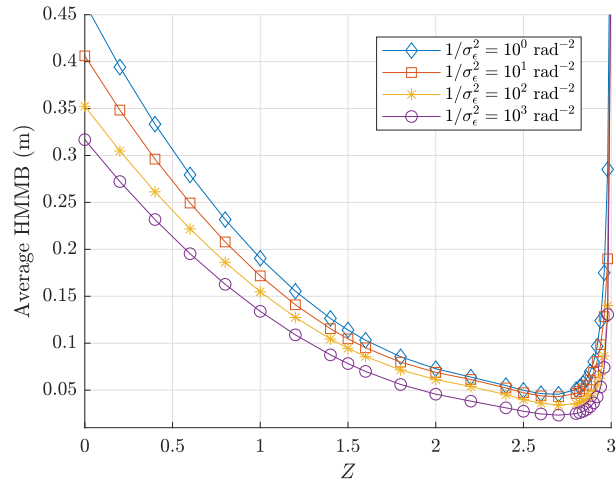
We observe that both the MML and AP1st estimators show an error floor for large SNR but due to different causes. The error floor of MML is due to the presence of the bias mentioned in Appendix A, caused by the inaccurate external orientation estimate, while that of AP1st is due to the inaccuracy of the first-order approximation. On the other hand, the RMSE of the position and orientation errors for the SPO and HyMM algorithms do not show an error floor. There, the RMSE for both types of errors reduces in inverse proportion to the SNR, i.e. the algorithms are able to estimate the position and orientation with high accuracy from the received optical signal. Next, we show in Figs. 7b and 7d the RMSE for positioning and orientation as a function of the number N_L of LEDs, for SNR = 35 dB. Also here, we see an asymptotic tightness between the RMSEs and their respective lower bounds. For a large number of LEDs, the RMSE and lower bound of the MML algorithm show an error floor, for the same reason as mentioned above. The results shown in Fig. 7 confirm that for large SNR or large N_L , the presence of the external estimate has no impact on the performance when the optical



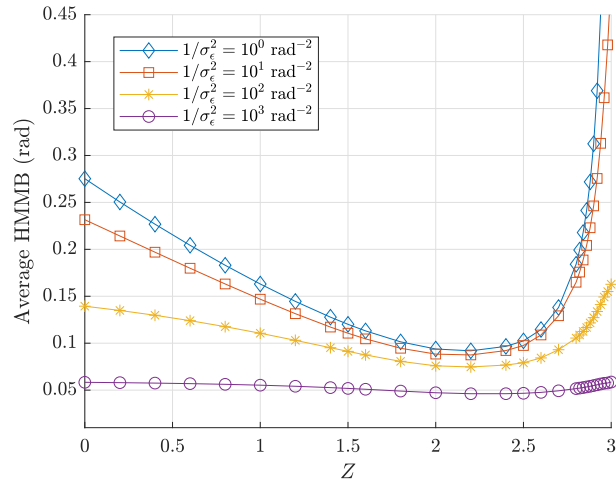
(a) Rooted bound on position error for the XY plane fixed at 1.5 m in z-axis



(c) Rooted bound on orientation error for the XY plane fixed at 1.5 m in z-axis



(b) The root of the bound on position error as a function of the height, averaged over the XY plane.



(d) The root of the bound on orientation error as a function of the height, averaged over the XY plane.

Fig. 8. The root of theoretical lower bound as a function of the position of the receiver.

signal contains sufficient information to accurately estimate the position and orientation from the optical signal, i.e. SPO and HyMM perform equally well. The improvement compared to the SPO algorithm is found when the optical signal is not sufficient to reliably estimate the orientation as well as the position, i.e. when there are not enough light sources to cover the whole area, or when the SNR is too small.

C. Impact of Location of the Receiver

In this section, we investigate the performance of the proposed receiver as a function of the position of the receiver. We consider the same room setup as illustrated in Fig. 3. Further, we assume the receiver is pointing upwards, the variance $1/\sigma_\epsilon^2 = 1 \times 10^2 \text{ rad}^{-2}$ and $\text{SNR} = 35 \text{ dB}$. In the first simulation, we assume the height of the receiver is fixed at $z = 1.5 \text{ m}$, i.e. at a vertical distance of 1.5 m from the floor, and compute the HCRB as a function of the position of the receiver in the XY plane. Figs. 8a and 8c show the

root of the HCRB, denoted as HMMB, for the position error and the orientation error, respectively. The HMMB has an inverted dome shape, where in the largest part of the area the HMMB is low and only shows some small fluctuations, and at the edges of the area, the HMMB is strongly degraded. This effect is due to the limited FOV of the receiver, as the closer the receiver is to the side boundary, the less LEDs it will sense. Next, we consider the effect of the vertical distance Z between the floor and the receiver. The root of the HRCB, i.e. HMMB, averaged over the XY plane, is shown as function of the vertical distance Z in Figs. 8b and 8d. As can be observed, when the height Z increases, the HMMB improves as the distance between the LEDs and the receiver reduces. However, because the incidence angles become relatively larger when the vertical distance between the LEDs and the receiver reduces, the incident angles may grow too large, implying the LEDs will starting to fall out of the FOV of the receiver. This explains the strong increase of the HMMB when the height approaches the maximum height of 3 m, although the effect

on the orientation HMMB is smaller, especially when more reliable prior information on the orientation is available.

VI. CONCLUSION

In this paper, we investigated RSS-based hybrid position and orientation estimation for a visible light system with multiple LEDs and multiple PDs in the presence of possibly unreliable prior information on the orientation. We first constructed the channel gain model of the multiple LEDs – multiple PDs system and the discussed the model used for the orientation uncertainty. We designed a RSS-based position and orientation estimation algorithm based on the hybrid ML/MAP principle, converted the optimization problem into a NLS problem and solved it with an iterative algorithm based on the Gauss-Newton method on manifolds. To investigate the optimality of the proposed estimator, we derived the theoretical lower bound for the hybrid ML/MAP estimator. We verified that the RMSE of the proposed estimator asymptotically approaches this theoretical bound for sufficiently large SNR and number of LEDs. Further, we also compared the performance of the proposed estimator with three state-of-the-art estimators, i.e., the SPO, the MML and the AP1st estimator, and found that, by properly exploiting the prior information on orientation, the proposed estimator performs well over the whole range of the orientation uncertainty, in contrast to the other estimators.

APPENDIX A

THEORETICAL LOWER BOUND FOR MML ESTIMATOR

In this appendix, we derive the theoretical lower bound for the MML estimator, which will be used in the numerical results section for comparison. Taking into account that the MML algorithm considers the external orientation estimate $\tilde{\mathbf{R}}$ as the correct orientation, and ignores the orientation uncertainty, it considers a misspecified log-likelihood function to estimate the position. As a consequence, the RMSE for the resulting position estimate (for a given external orientation estimate $\tilde{\mathbf{R}}$) can be lower bounded by the misspecified CRB (MCRB) [23], which is given by

$$\text{MCRB}(\mathbf{r}; \tilde{\mathbf{R}}) = (\mathbf{M}_1(\hat{\mathbf{r}}))^{-1} \mathbf{M}_2(\hat{\mathbf{r}}) (\mathbf{M}_1(\hat{\mathbf{r}}))^{-1} + \text{Bias}(\hat{\mathbf{r}}, \mathbf{r}), \quad (28)$$

where the position estimate is defined as

$$\hat{\mathbf{r}} = \arg \min_{\mathbf{r}} \left(D \left(p(\mathbf{y}|\Theta) \parallel p_m(\mathbf{y}|\mathbf{r}; \tilde{\mathbf{R}}) \right) \right). \quad (29)$$

In (29), $p(\mathbf{y}|\Theta)$ is the true PDF of \mathbf{y} where the conditioning is done on the correct position \mathbf{r} and orientation \mathbf{R} , $p_m(\mathbf{y}|\mathbf{r}; \tilde{\mathbf{R}})$ is the misspecified PDF of \mathbf{y} conditioned on the true position \mathbf{r} and parameterized by the (noisy) external orientation estimate $\tilde{\mathbf{R}}$, and $D \left(p(\mathbf{y}|\Theta) \parallel p_m(\mathbf{y}|\mathbf{r}; \tilde{\mathbf{R}}) \right)$ is the Kullback-Leibler divergence (KLD) between the true and the misspecified PDFs. The matrices \mathbf{M}_1 , \mathbf{M}_2 , and $\text{Bias}(\hat{\mathbf{r}}, \mathbf{r})$ are respectively given by

$$\mathbf{M}_1(\hat{\mathbf{r}}) = E_{\mathbf{y}|\Theta} \left\{ \nabla_{\mathbf{r}} \nabla_{\mathbf{r}}^T \ln p_m(\mathbf{y}|\hat{\mathbf{r}}; \tilde{\mathbf{R}}) \right\} \quad (30)$$

$$\mathbf{M}_2(\hat{\mathbf{r}}) = E_{\mathbf{y}|\Theta} \left\{ \nabla_{\mathbf{r}} \ln p_m(\mathbf{y}|\hat{\mathbf{r}}; \tilde{\mathbf{R}}) \nabla_{\mathbf{r}}^T \ln p_m(\mathbf{y}|\hat{\mathbf{r}}; \tilde{\mathbf{R}}) \right\} \quad (31)$$

$$\text{Bias}(\hat{\mathbf{r}}, \mathbf{r}) = (\mathbf{r} - \hat{\mathbf{r}}) (\mathbf{r} - \hat{\mathbf{r}})^T. \quad (32)$$

As in general, $p(\mathbf{y}|\Theta) \neq p_m(\mathbf{y}|\mathbf{r}; \tilde{\mathbf{R}})$, the matrices \mathbf{M}_1 and \mathbf{M}_2 are in general not equal [23]. The lower bound (28) still depends on the random variable $\tilde{\mathbf{R}}$. To obtain the lower bound on the RMSE of the position estimate, we therefore need to average (28) over the distribution of $\tilde{\mathbf{R}}$:

$$E\{\mathbf{r}_e \mathbf{r}_e^T\} \succeq E_{\tilde{\mathbf{R}}|\mathbf{R}}\{\text{MCRB}(\mathbf{r}; \tilde{\mathbf{R}})\}. \quad (33)$$

Note that the MML estimator does not estimate the orientation based on the optical signal. As a consequence, the mean squared error on the orientation is determined by the statistics of the prior distribution, i.e. $E\{\mathbf{u}_e \mathbf{u}_e^T\} = \Sigma_e$.

APPENDIX B FORMULAE

The Jacobian $\nabla_{\mathbf{R}} \epsilon$ is derived by [20], [35], [47] introducing an infinitesimal perturbation of $\exp(\mathbf{u}^\wedge)$ to \mathbf{R} in the equality of $\epsilon = -\log(\mathbf{R}\tilde{\mathbf{R}}^T)^\vee$ and calculating the limit with respect to \mathbf{u} , that is,

$$\begin{aligned} \nabla_{\mathbf{R}} \epsilon &\triangleq \frac{\partial}{\partial \mathbf{u}} \Big|_{\mathbf{u}=0} \left\{ -\log(\exp(\mathbf{u}^\wedge) \mathbf{R} \tilde{\mathbf{R}}^T)^\vee \right\} \\ &= \frac{\partial}{\partial \mathbf{u}} \Big|_{\mathbf{u}=0} \left\{ -\mathbf{J}^{-1}(-\epsilon) \mathbf{u} + \epsilon \right\} \\ &= -\mathbf{J}^{-1}(-\epsilon) \end{aligned} \quad (34)$$

where the penultimate equality holds because of the properties of the Baker-Campbell-Hausdorff (BCH) formula [35], and $\mathbf{J}^{-1}(\epsilon)$, referring to [35], is

$$\mathbf{J}^{-1}(\epsilon) = \frac{\|\epsilon\|}{2} \cot \frac{\|\epsilon\|}{2} \mathbf{I}_3 + \left(1 - \frac{\|\epsilon\|}{2} \cot \frac{\|\epsilon\|}{2} \right) \frac{\epsilon \epsilon^T}{\|\epsilon\|^2} - \frac{\epsilon^\wedge}{2}. \quad (35)$$

Then we have $|\det(\nabla_{\mathbf{R}} \epsilon)| = |\det(\mathbf{J}(-\epsilon))|^{-1}$, which is given by [35]

$$\begin{aligned} |\det(\nabla_{\mathbf{R}} \epsilon)| &= \frac{\|\epsilon\|^2}{2(1 - \cos \|\epsilon\|)} \\ &= \frac{1}{1 - \frac{\|\epsilon\|^2}{4!/2} + \frac{\|\epsilon\|^4}{6!/2} - \frac{\|\epsilon\|^6}{8!/2} + \dots} \end{aligned} \quad (36)$$

The Taylor expansion in the last equality shows that the limit of $|\det(\nabla_{\mathbf{R}} \epsilon)|$ for $\epsilon \rightarrow 0$ is equal to 1.

The expression of $\nabla_{\Theta} h_{i,j}$ is found in [20], and for completeness, it is included in this paper, which is

$$\begin{aligned} \nabla_{\Theta} h_{i,j} &= C_{i,j} \\ &\cdot \begin{bmatrix} \frac{\gamma (\mathbf{n}_i^T \mathbf{v}_{i,j})^{\gamma-1} (\mathbf{n}_{P,j}^T \mathbf{v}_{i,j})}{\|\mathbf{v}_{i,j}\|^{\gamma+3}} \\ \frac{(\mathbf{n}_i^T \mathbf{v}_{i,j})^\gamma}{\|\mathbf{v}_{i,j}\|^{\gamma+3}} \\ - \frac{(\gamma+3) (\mathbf{n}_i^T \mathbf{v}_{i,j})^\gamma (\mathbf{n}_{P,j}^T \mathbf{v}_{i,j})}{\|\mathbf{v}_{i,j}\|^{\gamma+5}} \end{bmatrix}^T \end{aligned}$$

$$\cdot \begin{bmatrix} \mathbf{n}_i^T, & \mathbf{n}_i^T (\mathbf{d}_j^\wedge)^T \\ \mathbf{n}_{P,j}^T, & \mathbf{v}_i^T (\mathbf{n}^\wedge)^T \\ \mathbf{v}_{i,j}^T, & \mathbf{v}_i^T (\mathbf{d}_j^\wedge)^T \end{bmatrix}. \quad (37)$$

The expression of $\nabla_{\mathbf{R}} \ln p(\mathbf{R}|\tilde{\mathbf{R}})$ is

$$\begin{aligned} \nabla_{\mathbf{R}} \ln p(\mathbf{R}|\tilde{\mathbf{R}}) \\ = -\epsilon^T \left(\frac{\|\epsilon\| \sin \|\epsilon\| - 2(1 - \cos \|\epsilon\|)}{\|\epsilon\|^2 (1 - \cos \|\epsilon\|)} \mathbf{I}_3 + \Sigma_\epsilon^{-1} \right) \nabla_{\mathbf{R}} \epsilon. \end{aligned} \quad (38)$$

REFERENCES

- [1] C.-X. Wang *et al.*, "Cellular architecture and key technologies for 5G wireless communication networks," *IEEE Commun. Mag.*, vol. 52, no. 2, pp. 122–130, Feb. 2014.
- [2] M. Ayyash *et al.*, "Coexistence of WiFi and LiFi toward 5G: Concepts, opportunities, and challenges," *IEEE Commun. Mag.*, vol. 54, no. 2, pp. 64–71, Feb. 2016.
- [3] E. C. Strinati, S. Barbarossa, J. L. Gonzalez-Jimenez, D. Ktenas, N. Cassiau, L. Maret, and C. Dehos, "6G: The next frontier: From holographic messaging to artificial intelligence using subterahertz and visible light communication," *IEEE Veh. Technol. Mag.*, vol. 14, no. 3, pp. 42–50, Sep. 2019.
- [4] N. Ul Hassan, A. Naeem, M. A. Pasha, T. Jadoon, and C. Yuen, "Indoor positioning using visible LED lights: A survey," *ACM Comput. Surv.*, vol. 48, no. 2, pp. 20:1–20:32, 2015.
- [5] Q. Wang *et al.*, "Light positioning: A high-accuracy visible light indoor positioning system based on attitude identification and propagation model," *Int. J. Distrib. Sensor Netw.*, vol. 14, no. 2, Feb. 2018, Art. no. 155014771875826.
- [6] P. Huynh and M. Yoo, "VLC-based positioning system for an indoor environment using an image sensor and an accelerometer sensor," *Sensors*, vol. 16, no. 6, p. 783, 2016.
- [7] B. Lin, Z. Ghassemlooy, C. Lin, X. Tang, Y. Li, and S. Zhang, "An indoor visible light positioning system based on optical camera communications," *IEEE Photon. Technol. Lett.*, vol. 29, no. 1, pp. 579–582, Apr. 1, 2017.
- [8] R. Zhang, W.-D. Zhong, K. Qian, and D. Wu, "Image sensor based visible light positioning system with improved positioning algorithm," *IEEE Access*, vol. 5, pp. 6087–6094, 2017.
- [9] A. şahin, Y. S. Eroğlu, İ. Güvenc, N. Pala, and M. Yüksel, "Hybrid 3-D localization for visible light communication systems," *J. Lightw. Technol.*, vol. 33, no. 22, pp. 4589–4599, Nov. 15, 2015.
- [10] H. Steendam, T. Q. Wang, and J. Armstrong, "Theoretical lower bound for indoor visible light positioning using received signal strength measurements and an aperture-based receiver," *J. Lightw. Technol.*, vol. 35, no. 2, pp. 309–319, Jan. 15, 2017.
- [11] W. Xu, J. Wang, H. Shen, H. Zhang, and X. You, "Indoor positioning for multiphotodiode device using visible-light communications," *IEEE Photon. J.*, vol. 8, no. 1, pp. 1–11, Feb. 2016.
- [12] H. Steendam, "A 3-D positioning algorithm for AOA-based VLP with an aperture-based receiver," *IEEE J. Sel. Areas Commun.*, vol. 36, no. 1, pp. 23–33, Jan. 2018.
- [13] X. Yu, J. Wang, and H. Lu, "Single LED-based indoor positioning system using multiple photodetectors," *IEEE Photon. J.*, vol. 10, no. 6, pp. 1–8, Dec. 2018.
- [14] S. H. Yang, E. M. Jeong, D. R. Kim, H. S. Kim, Y. H. Son, and S. K. Han, "Indoor three-dimensional location estimation based on LED visible light communication," *Electron. Lett.*, vol. 49, no. 1, pp. 54–56, Jan. 2013.
- [15] H.-S. Kim, D.-R. Kim, S.-H. Yang, Y.-H. Son, and S.-K. Han, "An indoor visible light communication positioning system using a RF carrier allocation technique," *J. Lightw. Technol.*, vol. 31, no. 1, pp. 134–144, Jan. 1, 2013.
- [16] H. Huang, L. Feng, P. Guo, A. Yang, and G. Ni, "Iterative positioning algorithm to reduce the impact of diffuse reflection on an indoor visible light positioning system," *Opt. Eng.*, vol. 55, no. 6, Jun. 2016, Art. no. 066117.
- [17] B. Zhou, V. Lau, Q. Chen, and Y. Cao, "Simultaneous positioning and orientating for visible light communications: Algorithm design and performance analysis," *IEEE Trans. Veh. Technol.*, vol. 67, no. 12, pp. 11790–11804, Dec. 2018.
- [18] B. Zhou, A. Liu, and V. Lau, "Joint user location and orientation estimation for visible light communication systems with unknown power emission," *IEEE Trans. Wireless Commun.*, vol. 18, no. 11, pp. 5181–5195, Nov. 2019.
- [19] B. Zhou, A. Liu, and V. Lau, "On the fundamental performance limit of visible light-based positioning," in *Proc. 13th Int. Conf. Signal Process. Commun. Syst. (ICSPCS)*, Dec. 2019, pp. 1–6.
- [20] S. Shen, S. Li, and H. Steendam, "Simultaneous position and orientation estimation for visible light systems with multiple LEDs and multiple PDs," *IEEE J. Sel. Areas Commun.*, vol. 38, no. 8, pp. 1866–1879, Aug. 2020.
- [21] E.-M. Jeong, S.-H. Yang, H.-S. Kim, and S.-K. Han, "Tilted receiver angle error compensated indoor positioning system based on visible light communication," *Electron. Lett.*, vol. 49, no. 14, pp. 890–892, Jul. 2013.
- [22] Q.-L. Li, J.-Y. Wang, T. Huang, and Y. Wang, "Three-dimensional indoor visible light positioning system with a single transmitter and a single tilted receiver," *Opt. Eng.*, vol. 55, no. 10, 2016, Art. no. 106103.
- [23] S. Fortunati, F. Gini, M. S. Greco, and C. D. Richmond, "Performance bounds for parameter estimation under misspecified models: Fundamental findings and applications," *IEEE Signal Process. Mag.*, vol. 34, no. 6, pp. 142–157, Nov. 2017.
- [24] B. Zhou, A. Liu, and V. Lau, "Performance limits of visible light-based user position and orientation estimation using received signal strength under NLOS propagation," *IEEE Trans. Wireless Commun.*, vol. 18, no. 11, pp. 5227–5241, Nov. 2019.
- [25] S. Li, S. Shen, and H. Steendam, "A positioning algorithm for VLP in the presence of orientation uncertainty," *Signal Process.*, vol. 160, pp. 13–20, Jul. 2019.
- [26] H. Van Trees, K. Bell, and Z. Tian, "Detection estimation modulation theory—Part I: Detection, estimation, filtering theory," in *Detection Estimation and Modulation Theory*. Hoboken, NJ, USA: Wiley, 2013.
- [27] Y. Noam and H. Messer, "Notes on the tightness of the hybrid Cramér–Rao lower bound," *IEEE Trans. Signal Process.*, vol. 57, no. 6, pp. 2074–2084, Jun. 2009.
- [28] J. M. Kahn and J. R. Barry, "Wireless infrared communications," *Proc. IEEE*, vol. 85, no. 2, pp. 265–298, Feb. 1997.
- [29] M. Biagi, A. M. Vegni, and T. D. C. Little, "LAT indoor MIMO-VLC—Localize, access and transmit," in *Proc. Int. Workshop Opt. Wireless Commun. (IWOW)*, Oct. 2012, pp. 1–3.
- [30] S. Pergoloni, Z. Mohamadi, A. M. Vegni, Z. Ghassemlooy, and M. Biagi, "Metameric indoor localization schemes using visible lights," *J. Lightw. Technol.*, vol. 35, no. 14, pp. 2933–2942, Jul. 15, 2017.
- [31] T. Komine and M. Nakagawa, "Fundamental analysis for visible-light communication system using LED lights," *IEEE Trans. Consum. Electron.*, vol. 50, no. 1, pp. 100–107, Feb. 2004.
- [32] M. F. Keskin, S. Gezici, and O. Arikan, "Direct and two-step positioning in visible light systems," *IEEE Trans. Commun.*, vol. 66, no. 1, pp. 239–254, Jan. 2018.
- [33] Y. Zhuang, L. Hua, L. Qi, J. Yang, P. Cao, Y. Cao, Y. Wu, J. Thompson, and H. Haas, "A survey of positioning systems using visible LED lights," *IEEE Commun. Surveys Tuts.*, vol. 20, no. 3, pp. 1963–1988, 3rd Quart., 2018.
- [34] J. J. Craig, *Introduction to Robotics: Mechanics and Control*, 3/E. London, U.K.: Pearson, 2009.
- [35] T. D. Barfoot, *State Estimation for Robotics*. Cambridge, U.K.: Cambridge Univ. Press, 2017.
- [36] L. Falorsi, P. de Haan, T. R. Davidson, and P. Forré, "Reparameterizing distributions on Lie groups," in *Proc. 22nd Int. Conf. Artif. Intell. Statist.*, 2019, pp. 3244–3253.
- [37] T. D. Barfoot and P. T. Furgale, "Associating uncertainty with three-dimensional poses for use in estimation problems," *IEEE Trans. Robot.*, vol. 30, no. 3, pp. 679–693, Jun. 2014.
- [38] E. Eade. (May 2017). *Lie Groups for 2D and 3D Transformations*. [Online]. Available: <http://ethaneade.com/lie.pdf>
- [39] A. Yeredor, "The joint MAP-ML criterion and its relation to ML and to extended least-squares," *IEEE Trans. Signal Process.*, vol. 48, no. 12, pp. 3484–3492, Dec. 2000.
- [40] S. M. Kay, *Fundamentals Stat. Signal Processing: Estimation Theory*. Upper Saddle River, NJ, USA: Prentice-Hall, 1993.
- [41] C. P. Robert and G. Casella, *Monte Carlo Statistical Methods*, vol. 2. Springer, 1999.
- [42] S. H. Yang, H. S. Kim, Y. H. Son, and S. K. Han, "Three-dimensional visible light indoor localization using AOA and RSS with multiple optical receivers," *J. Lightw. Technol.*, vol. 32, no. 14, pp. 2480–2485, Jul. 15, 2014.

- [43] A. Nuwanpriya, S.-W. Ho, and C. S. Chen, "Indoor MIMO visible light communications: Novel angle diversity receivers for mobile users," *IEEE J. Sel. Areas Commun.*, vol. 33, no. 9, pp. 1780–1792, Sep. 2015.
- [44] C. Chen, W.-De Zhong, H. Yang, S. Zhang, and P. Du, "Reduction of SINR fluctuation in indoor multi-cell VLC systems using optimized angle diversity receiver," *J. Lightw. Technol.*, vol. 36, no. 17, pp. 3603–3610, Sep. 1, 2018.
- [45] L. Zeng *et al.*, "High data rate multiple input multiple output (MIMO) optical wireless communications using white led lighting," *IEEE J. Sel. Areas Commun.*, vol. 27, no. 9, pp. 1654–1662, Dec. 2009.
- [46] S. Cincotta, C. He, A. Neild, and J. Armstrong, "High angular resolution visible light positioning using a quadrant photodiode angular diversity aperture receiver (QADA)," *Opt. Exp.*, vol. 26, no. 7, pp. 9230–9242, 2018.
- [47] C. J. Taylor and D. J. Kriegman, "Minimization on the Lie group $SO(3)$ and related manifolds," Yale Univ., New Haven, CT, USA, Tech. Rep. 9405, 1994.



Shengqiang Shen received the B.S. degree in information engineering from the China University of Mining and Technology, Xuzhou, China, in 2013, and the Ph.D. degree in electrical engineering from Ghent University, Ghent, Belgium, in 2021. He is currently a Lecturer with the School of Information and Control Engineering, China University of Mining and Technology. His research interests include visible light positioning and wireless communication.



Shiyin Li received the Ph.D. degree in information and communication engineering from the China University of Mining and Technology, Xuzhou, China, in 2010. Since 2010, he has been a Professor with the School of Information and Control Engineering, China University of Mining and Technology. He is currently the Vice Dean of the School of Information and Control Engineering. His research interests include wireless communication and indoor localization.



Heidi Steendam (Senior Member, IEEE) received the M.Sc. degree in electrical engineering and the Ph.D. degree in applied sciences from Ghent University, Ghent, Belgium, in 1995 and 2000, respectively.

Since September 1995, she has been with the Digital Communications (DIGCOM) Research Group, Department of Telecommunications and Information Processing (TELIN), Faculty of Engineering, Ghent University, first in the framework of various research projects and since October 2002 as a Professor in the area of digital communications. She was a Visiting Professor at Monash University in 2015 and at ESPOL in 2019. She is the author of more than 150 scientific papers in international journals and conference proceedings, for which several best paper awards were received. Her main research interests are in statistical communication theory, carrier and symbol synchronization, bandwidth-efficient modulation and coding, cognitive radio and cooperative networks, and positioning and visible light communication. Since 2002, she has been an Executive Committee Member of the IEEE Communications and Vehicular Technology Society Joint Chapter, Benelux Section, and later as the Vice Chair since 2012 and the Chair since 2017. She was active in various international conferences as a technical program committee chair or Technical Program Committee Member and the session chair. In 2004 and 2011, she was the Conference Chair of the IEEE Symposium on Communications and Vehicular Technology, Benelux. From 2012 to 2017, she was an Associate Editor of *IEEE TRANSACTIONS ON COMMUNICATIONS* and *EURASIP Journal on Wireless Communications and Networking*.